The freezing process of small lipid vesicles at molecular resolution

Risselada, H. Jelger; Marrink, Siewert J.

Published in:
Soft Matter

DOI:
10.1039/b913210d

The freezing process of small lipid vesicles at molecular resolution†

H. Jelger Risselada and Siewert J. Marrink*

Received 3rd July 2009, Accepted 28th August 2009
First published as an Advance Article on the web 25th September 2009
DOI: 10.1039/b913210d

At present very little is known about the kinetic barriers which a small vesicle will face during the transformation from the liquid-crystalline to the gel phase, and what the structure of frozen vesicles looks like at the molecular level. The formation of gel domains in the strongly curved bilayer of a small vesicle seems almost paradoxical and is expected to involve large structural reorganizations. In this work we use coarse-grained molecular dynamics simulations to study the kinetic and structural aspects of gel domain formation in small lipid vesicles, specifically dipalmitoylphosphatidylcholine (DPPC) vesicles with a diameter range of 20–40 nm. We observe that cooling of such vesicles below the phase transition temperature does not result in gel phase formation on a microsecond time scale, which we attribute to the presence of an effective area constraint. This area constraint is due to the strongly reduced membrane permeability at lower temperatures, preventing the rapid efflux of water and the required decrease in membrane area to form a gel phase. Control simulations with lamellar bilayers, simulated at fixed area, show that gel phase formation is indeed only possible below a certain threshold area. The effect of lipid asymmetry was also studied with the lamellar setup, and found to be of less importance. To circumvent the kinetic barrier imposed by the effective area constraint of the liposomes, *i.e.* to mimic the long time behavior, we introduce artificial pores in the membrane facilitating the solvent efflux. In this case, spontaneous gel domains are formed. We identify several stages during the microsecond-long transformation, finally resulting in strongly deformed or ruptured vesicles entirely in the gel state.

1 Introduction

Liposomes, *i.e.* tiny lipid vesicles, play an important role in many biological processes such as membrane fusion, fission and transport. They are also widely used in biotechnological applications, notably drug delivery. In biophysical studies, artificial liposomes are often used to mimic cells or cellular bodies. Obviously, the curvature of the liposomal membrane affects its properties compared to the lamellar state, and the properties become curvature-dependent. For instance, the main phase transition temperature T_m is found to decrease gradually with decreasing vesicle size for vesicles smaller than ~70 nm in diameter.[1,2] Especially in the limit of high curvature (small vesicles), the formation of gel domains is strongly suppressed, which is directly related to the strong increase in bending modulus of gel membranes with respect to membranes in a liquid-crystalline state. In some cases, this may cause freeze-induced fusion or rupture of small vesicles.[3] The cooling of vesicles is furthermore subject to a number of additional kinetic effects which are not present in lamellar systems, such as the efflux of interior water and the redistribution of lipids between the inner and outer monolayers.

Very little is in fact known about the mechanisms of gel domain formation in vesicles at a molecular level of detail. Particle-based simulation models offer a useful tool to provide this information. Lipid phase transitions have already been studied computationally in planar model membrane patches, providing insight to the kinetic factors of domain formation[4] and to the structural organization of the lipids in the gel phase.[4–9] Simulation studies of lipid vesicles have also been increasingly reported, focussing on their self-assembly, structure, and fusogenic properties.[10–15] To date, a few computational studies have been reported concerning phase transitions of lipid liposomes.[16–18] These studies, however, deal with liquid–liquid phase separation in multi-component vesicles.

In this article, we focus on a more detailed description of the transformation from the liquid-crystalline to the gel phase of small, single-component, DPPC vesicles. We use the Martini coarse-grained (CG) force field,[19,20] which has been successfully applied to the study of lipid polymorphism.[4,21,18] The use of a CG force field allows simulations to be extended to the microsecond time scale, whereas atomistic studies of vesicles are limited to nanoseconds,[22,13] too short to study gel phase formation. The simulations described in this work are divided in to three parts. In the first part, we consider vesicles that are instantaneously cooled below T_m. We analyze the induced stress in the liposomal membrane using our recently developed method to calculate the 3D pressure field across the system.[23] The kinetic barriers for lipid flip-flop and solvent exchange prevent these vesicles forming gel domains on the time scale of our simulations. In the second section of this work, we investigate the general effects of area constraints and lipid asymmetry on the formation of gel domains in lamellar systems, *i.e.* in the absence of curvature. In the last section, we mimic the slow, near-equilibrium, cooling of the vesicles. This is achieved by incorporating artificial pores that

Groningen Biomolecular Sciences and Biotechnology Institute & Zernike Institute for Advanced Materials, University of Groningen, Nijenborgh 4, 9747 AG Groningen, The Netherlands. E-mail: S.J.Marrink@rug.nl
† This paper is part of a *Soft Matter* themed issue on Modelling of soft matter. Guest editor: Mark Wilson.

allow both lipid flip-flops and solvent exchange. The formation of gel domains is now observed, and described in detail. However, before the results are presented and discussed, we describe the methodology used in this work.

2 Methods

2.1 Vesicular systems

Vesicles of three different sizes were studied, consisting of 2528, 5915 and 10529 DPPC lipids with an approximate diameter of 20, 30, and 40 nm, respectively. The initial temperature of the vesicular systems was $T = 323$ K, above the experimental $T_m = 315$ K for DPPC lipids. All vesicles were formed by a spontaneous aggregation process, using the MFFA (Mean Field Force Approximation) boundary approach recently developed in our group.[24] In the MFFA approach, the liposome is embedded in a spherical shell consisting of explicit solvent. Excess solvent is efficiently replaced by the action of the MFFA boundary, leading to an obvious computational advantage. Importantly, the MFFA boundary also helps to form liposomes of a desired size from spontaneous aggregation on very short timescales. Thus, starting from a random mixture of lipids and solvents, vesicles were formed on a time scale of 20–50 ns. However, in our previous work[24,15] we demonstrated that vesicles, once sealed, are likely not fully equilibrated. The vesicular membrane remains under expansive stress as a consequence of the line tension that surrounds it, right up to the moment of closure of the final pore. The total membrane area is therefore too large, and the vesicle formed too big in comparison to the expected equilibrium state. A similar conclusion was also reached recently in the work of Markvoort *et al.*[25] To equilibrate the vesicles, we introduced a repulsive harmonic potential (with force constant 50 kJ mol^{-1} nm^{-1}) of cylindrical symmetry, which only acts on the carbon tails of the lipids. These potentials induce toroidal pores in the liposomal membrane, which allow both the internal solvent (pressure difference) and the population of lipids over the monolayers to equilibrate. As the length along the cylindrical boundary is infinite, two pores occur in the vesicle. In the smallest, 20 nm diameter, vesicle a potential was introduced with a radius of 1.5 nm; in the larger vesicles potentials were added with a radius of 3.5 nm. The cylindrical boundaries were present from the start of the self-assembly process. More details about the MFFA boundary approach and the use of auxiliary cylindrical potentials can be found in the original publication.[24] Vesicles were considered equilibrated when net drift in lipid flip-flops and water flux no longer occurred. Equilibration took 400, 200, and 260 ns for the vesicles of sizes 20, 30, and 40 nm, respectively.

After the equilibration of the vesicles at $T = 323$ K, two sets of cooling simulations were performed. In the first set, the cylindrical potentials were removed and the liposomal matrix allowed to seal, after which the vesicles were instantaneously cooled to a temperature of 273 K, well below T_m. Note that the CG Martini force field underestimates the phase transition temperature somewhat (for a CG lamellar DPPC membrane, T_m is 295 ± 5 K[4]), necessitating the large temperature drop. During the subsequent simulations of 0.2–1 μs, no gel formation was observed in this series of simulations, which we attributed to the non-equilibrium nature of the instantaneous cooling process, as will be discussed in the Results section. To allow the vesicles to equilibrate at the lowered temperature, a second set of simulations was performed. Here, the artificial pores used for the equilibration of the vesicles were retained during the subsequent simulation of 0.3–1.6 μs at 273 K. Table 1 summarizes the different vesicular system setups used in this study.

Table 1 Overview of vesicle simulations. Vesicle diameter, radius of the MFFA boundary potential (R_{MFFA}), amount of DPPC lipids and CG water beads, and total simulation time after equilibration, are listed

Diameter (nm)	R_{MFFA} (nm)	Amount of DPPC (nm)	No. of CG water beads[a]	Time[b] (ns)	
				Set 1[c]	Set 2[c]
20	15.0	2528	84 220	1000	1600
30	20.0	5915	200 844	600	800
40	23.0	10 529	288 184	200	300

[a] One CG water particle represents four real water molecules. [b] Here, and throughout the manuscript, an effective time is reported. Based on the increase in self-diffusion of lipids and water in the Martini model, the effective time was obtained by multiplication of the time axis by a factor of four.[19] [c] In set 1, the cylindrical potentials were removed after equilibration of the vesicles. In set 2, these potentials were kept to allow for solvent exchange and lipid flip-flops. See text for details.

2.2 Lamellar systems

In order to compare the effects observed for the vesicular systems, a number of bilayer systems consisting of 512 DPPC lipids were also simulated. The simulations were performed in the NAP_zT ensemble, with the area ranging from 0.45 to 1.0 nm^2 per lipid. Starting structures for these simulations were generated from an initially equilibrated bilayer at 323 K, which was quenched to 273 K under constant surface tension, allowing the area per lipid to adjust. Simulations at constant area were subsequently run for 400 ns, keeping the temperature at $T = 273$ K, and setting the normal pressure $P_z = 1$ bar. In addition, a series of asymmetric DPPC bilayers were prepared by systematic removal of a number of lipids from one of the two monolayers of a bilayer equilibrated at $T = 323$ K. These systems were also quenched to 273 K, and simulated for 800 ns at zero surface tension.

2.3 Simulation parameters

All simulations were performed using the Martini coarse-grained (CG) model, version 1.4, using the standard settings with respect to the use of cut-offs and shift functions.[19] An integration time step of 40 fs was used, corresponding to an effective time of 160 fs (see footnote of Table 1). Temperature of both the vesicular and bilayer systems were coupled to the Berendsen thermostat,[26] using $\tau_t = 1.0$ ps, with separate scaling of lipids and water. Pressure in the bilayer system was controlled using the Berendsen barostat,[26] with $\tau_p = 1.0$ ps and a compressibility of 5×10^5 bar^{-1}. In the case of zero surface tension conditions, coupling of the lateral and perpendicular dimensions was performed independently. For the pressure control in the vesicular systems we used a Langevin piston method as described in the next section. The software used to perform the simulations is Gromacs version

3.3.1,[27] modified to include both the MFFA–boundary and the Langevin piston method.

2.4 Langevin piston method

In contrast to the pressure on either side of a lamellar membrane, the pressure inside and outside a vesicle can differ. Such pressure differences will occur, for instance, under conditions of osmotic shock, but also as a result of a change in temperature. This poses a challenge for simulation studies, which usually define a global pressure based on the average virial in the system. The global pressure can be efficiently controlled by a number of coupling algorithms, but pressure differences cannot. Ideally, only the surroundings of the vesicle are coupled to the required reference pressure, while the interior of the vesicle is not affected by the coupling. Such coupling schemes would require a local definition and coupling of pressure. The most straightforward solution is to use the Langevin piston method[28] to couple the position of the MFFA boundary to the equations of motion:

$$m_{\mathrm{b}}\frac{\mathrm{d}v}{\mathrm{d}t} = F_{\mathrm{b}} - \frac{P_{\mathrm{ref}}}{A_{\mathrm{b}}} - \gamma v + R(t) \quad (1)$$

Here, m_{b} is the mass of the boundary piston, v is the velocity of the boundary, F_{b} is the force on the boundary coming from the particles, P_{ref} is the chosen reference pressure, γ is the friction coefficient, and $R(t)$ is a white noise random force. By definition, γ and $R(t)$ are related by the fluctuation dissipation theorem. The application of such coupling scheme under mean field boundary conditions has already been successfully demonstrated by Heller *et al.*[29]

To calibrate the boundary pistons for use in our vesicle studies, we used pure solvent systems embedded in a MFFA potential matching the size of the vesicles. The target of the calibration was an internal pressure of 1 bar in the bulk solvent. A friction coefficient $\gamma = 60\ \mathrm{ps}^{-1}$ and piston masses of $m_{\mathrm{b}} = 750, 1000, 1500$ amu nm^{-2} for the 20, 30, and 40 nm systems, respectively, resulted in a well-controlled pressure in which large pressure fluctuations were effectively damped.

2.5 Analysis details

2.5.1 Area per lipid. Due to the spherical shape of the vesicles, the area per lipid can not be uniquely defined as it can be for a lamellar system. Here we use the average position of the C2 tail beads of the lipids to define the area per lipid for the outer and inner monolayers of the vesicles. The C2 bead denotes the second tail bead with respect to the lipid head groups, and maps to carbons 5–8 of the corresponding palmitoyl chain. The C2 tail bead is close to the geometrical center of the DPPC lipid.

2.5.2 Detection of gel domains. To provide a quantitative estimate of the fraction of the gel phase in the membranes, we used a simple distance-based cluster algorithm on the second tail bead of DPPC (C2). An element (*i.e.* tail bead) belongs to a certain cluster when the distance to any one of the other elements in the cluster is smaller than D_{cut}. We found that the ideal cutoff distance D_{cut} for the cluster algorithm is 0.543 nm in the planar membrane and 0.570 nm in the vesicle. This ideal cutoff was determined by visualizing and matching the detected clusters from several snapshots. The slightly larger cutoff for the vesicular case is required due to the less regularly packed structure of the gel domains in the curved membrane. It is important to note, however, that the curvature in the vesicular systems changes during the phase transition; the cutoff used for vesicles is an averaged cutoff optimized to detect clusters across the entire trajectory. In vesicles, the results obtained with the present algorithm therefore only predict a trend. Using the cluster definition, gel domains are defined as follows: In the planar membrane, the biggest cluster corresponds to the gel domain (only one gel domain per monolayer is formed in the bilayer simulations), whereas in the vesicular membrane the gel domains are characterized by the set of clusters consisting of more than 10 lipids.

2.5.3 Solvent and lipid exchange. In order to count the amount of solvent beads inside the vesicle, two definitions were used. In the simulations performed in set 1, the vesicles are sealed, the number of internal solvent beads is obtained using a distance-based cluster algorithm using a cutoff of 0.8 nm between the water beads. Thus two large clusters are obtained, corresponding to the internal and external solvent. The cluster-based counting is also accurate when the vesicles undergo large shape deformations. In the case of set 2 simulations, and also during equilibration, the vesicles contain artificial pores and the two clusters can no longer be strictly separated. As a qualitative estimate, internal solvent was defined as those water beads that are located within the average radius of the vesicle. The average vesicle radius was calculated as the average distance of all lipid beads with respect to the geometrical center of the vesicle. Lipid flip-flops were characterized by identifying the location in the membrane of each lipid, *i.e.* inner *versus* outer monolayer, as a function of time. To prevent artifacts due to shape deformations, lipids were assigned to a certain monolayer by use of a distance based cluster algorithm (as previously described) on the glycerol-groups of the lipids using a cutoff criterion of 1.5 nm. All lipids within a buffer region of 4 nm radius located around the center of the artificial pores were excluded from the clustering. Using this definition exactly two clusters are found, representing each of the two monolayers. When a lipid was initially located in one monolayer and later appeared in the other monolayer, a flip-flop event was counted. Due to the existence of a buffer region at the pore interface which the lipids need to pass, the initial detection of flip-flop requires a certain lag-time.

2.5.4 Vesicle shape. To quantify the shape of the vesicle a quantity A_d called asphericity is used. Mathematically it is defined by:

$$A_{\mathrm{d}} = \frac{\sum_{i>j}\left\langle \left(\lambda_i - \lambda_j\right)^2 \right\rangle}{2\left\langle \left(\sum_{i=1}^{3}\lambda_i\right)^2 \right\rangle} \quad (2)$$

and it has zero as a lower bound for a spherical object. Here λ_1, λ_2, and λ_3, are the principal radii of gyration, given by the eigenvalues of the radius of gyration tensor.

2.5.5 Calculation of surface tension. Using our recently developed 3D pressure field method[23] as a post-analysis tool on

the simulation trajectory, we were able to measure the local pressures in the system. Making use of the spherical symmetry of the vesicle, the normal (= radial) P_N and lateral (= tangential) P_{LAT} components of the pressure are obtained as a function of the distance r from the vesicle center.[23] The surface tension in the curved vesicular membrane σ is computed using the mechanical approach reported by Thompson *et al.*,[30]

$$\sigma = \left[-\frac{(P_{out} - P_{in})^2}{8} \int_0^\infty r^3 \frac{dP_N(r)}{dr} dr \right]^{1/3} \quad (3)$$

where $P_{out} - P_{in} = \Delta P$ is the pressure difference over the vesicle membrane.

3 Results and discussion

3.1 Quenching vesicles below T_m

In this section we study the effect on vesicles of a sudden temperature quench from $T = 323$ K to $T = 273$ K, corresponding to a quench from the liquid-crystalline phase to the gel phase in the case of lamellar DPPC. The vesicles were allowed to fully equilibrate at the higher temperature, making use of artificial pores which were removed before the actual quenching to the lower temperature. Based on visual inspection as well as on the analysis of the biggest domains found with the cluster algorithm, none of the vesicles, with diameters of 20, 30, and 40 nm, showed any tendency toward gel formation over the entire simulation time (up to 2 μs for the smallest, including equilibration time). We will argue below that this is likely a kinetic effect caused by the restricted efflux of solvent, and show in detail the stress developing inside the quenched vesicles in their meta-stable fluid state.

3.1.1 Rapid cooling of vesicles imposes area constraint. For a gel phase to be able to form, the area of the liposome needs to shrink considerably. This can only happen if the internal volume decreases, that is upon release of internal solvent. In the absence of large structural defects, protein channels or pores, this requires passive permeation of water across the lipid membrane. Monitoring the amount of interior solvent during our simulations, we quantified this passive water flux for the 20 nm vesicle. Over a time scale of 100 ns, 15 flux events are observed, on average, at 323 K. Considering the large number of internal solvent beads (7115), flux events are rare. Even though the cooling of the vesicle causes an increased pressure gradient between the interior and exterior solvent (see below), a drastic decrease in water flux is observed when cooling the vesicle to 273 K. Not more than a handful of water molecules are observed to cross the membrane during the entire 1.6 μs simulation. Since water is also not very compressible (for a temperature decrease from 323 K to 273 K the density of the CG water decreases with 4% in the CG model; for real water this is around 1%), in practice this means that an area constraint is applied to the vesicular membrane. This effective area constraint is anticipated to be the reason for the stability of the fluid phase. The average area per lipid, based on the C2 tail bead, is 0.69 and 0.60 nm^2 at 273 K, for the inner and outer monolayers respectively, a decrease of only 3.4% and 2.6% compared to the area per lipid of 0.71 and 0.62 nm^2 at 323 K.

The question remains why the permeability of the membrane decreases so much. Previously we have shown that the water permeability coefficient of a DPPC vesicle at 323 K is of the order of 10^{-3} cm s^{-1},[10] in agreement with experimental measurements.[31,32] Experimental measurements also show a large decrease of the water permeability for vesicles below T_m. Cooling of DPPC membranes from 10 K above T_m to 10 K below T_m, the permeability is observed to decrease by a factor of 100,[31] which is usually attributed to the increased packing of the lipid tails in the gel phase. However, in our simulations the vesicles are still in a fluid phase. There are several factors that might contribute to the reduced permeability of this fluid phase. First, the area per lipid has decreased slightly, due to the small but non-zero water compressibility. Second, assuming an Arrhenius temperature dependence of the permeation rate, the temperature difference (50 K) reduces the rate approximately fivefold. Third, the activation energy for the permeation process is expected to be temperature-dependent. Based on temperature-dependence data[33] for water solubility in apolar solvents, one expects a substantial increase in the activation barrier. Taken together, these factors can easily account for the low permeation rate of the supercooled vesicles, putting the membrane under stress and preventing the formation of gel domains. Before testing this hypothesis by looking at gel formation in planar bilayers under stress, first we analyze the stress distribution of the vesicles in more detail.

3.1.2 Cooling stresses the liposomal membrane. The stress distribution across the vesicular systems, obtained from the radially averaged 3D pressure field (see Methods), is shown in Fig. 1. Some of the properties derived from these profiles, namely the radius, the pressure difference between the inside and outside of the vesicles, and the tension of the vesicular membrane are summarized in Table 2. Fig. 1A compares the pressure profile of a 20 nm diameter vesicle either in a relaxed state at 323 K or in a stressed state at 273 K. Both profiles show the characteristic pattern also observed in lamellar systems: two regions of positive pressure located near the lipid head groups, two regions of negative pressure at the lipid tail–water interface, and a central region of positive pressure inside the hydrophobic membrane core. We refer to previous work for a more detailed discussion about the comparison between lamellar and vesicular pressure profiles.[23] Of interest here is the appearance of a clear pressure difference between the interior and exterior solvent for the cooled vesicle (showing up in the normal P_N and lateral P_{LAT} components of the pressure profile). The pressure difference exceeds 60 bar, for each of the three vesicle sizes studied (*cf.* Table 2). As a consequence of the interior pressure, the vesicular membrane is under considerable tension. To quantify these surface tensions, we used eqn (3). The resulting tensions are summarized in Table 2. The surface tension of the cooled vesicular membrane is of the order of 30–45 mN m^{-1}. The error in these numbers is almost 10 mN m^{-1}, and prevents drawing conclusions with respect to the different sizes of the vesicles. It is of interest to compare the magnitude of the tension observed in our cooled vesicles to the rupture tension of vesicles determined experimentally. In general, lipid bilayers are known to rupture under tensions of the order of 1–5 mN m^{-1}. Based on these numbers one would expect our simulated vesicles to have ruptured already. However,

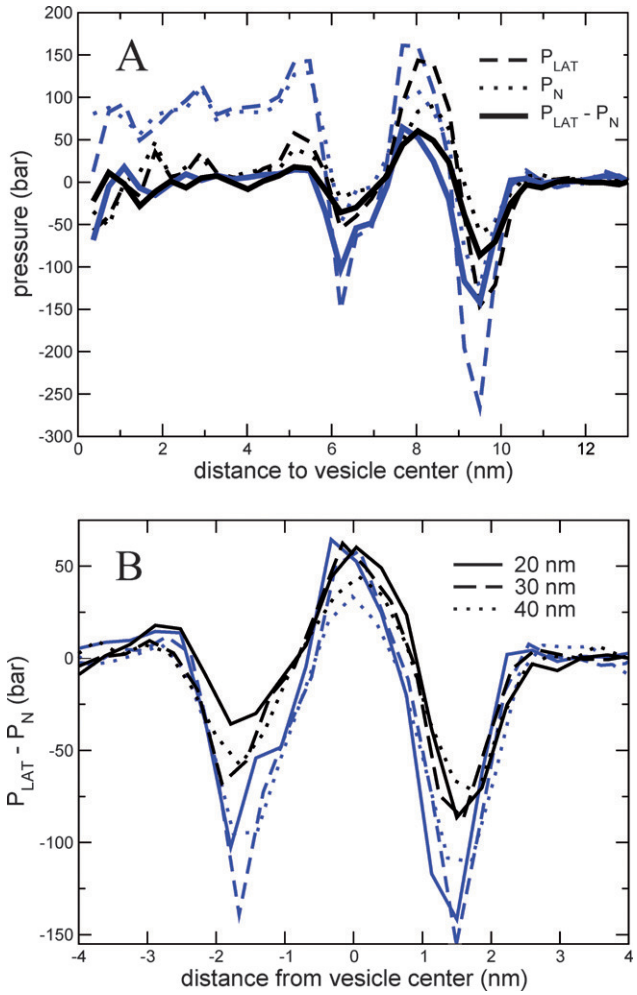

Fig. 1 Pressure distributions for vesicular systems. (A) Lateral (P_{LAT}), normal (P_N), and differential ($P_{LAT} - P_N$) pressure distribution across a 20 nm vesicle. Black lines represent the profiles at 323 K and blue lines at 273 K. (B) Differential pressure profiles ($P_{LAT} - P_N$) of the three differently sized vesicles, both at 323 K (black lines) and 273 K (blue lines). The profiles are centered with respect to the center of the membrane.

rupture is a dynamic process and depends strongly on the rate at which loading is applied.[34] On the short time scale of our simulations one expects therefore the membrane to be more stable, requiring a much larger tension before spontaneous rupture is observed. In line with this expectation, simulation studies of lamellar bilayers[35] have shown that spontaneous rupture is only observed for tensions exceeding 90 mN m^{-1}.

Note that, also at 323 K, the vesicular membrane is not in a completely tension-less state, especially considering the two bigger vesicles. In fact, it is surprisingly difficult to fully equilibrate the vesicles. The cylindrical potentials used to equilibrate the internal pressure in the vesicle need to be rather large (3.5 nm radius) to allow for sufficient lipid flip-flops. After their removal, sealing of these pores takes place within a few nanoseconds. Within such a short time scale this sealing is achieved by expanding the area of the membrane, rather than by decreasing the internal volume of the vesicle. This results in a small remaining tension. We should therefore keep in mind that the presence of this initial tension gives a bias in the interpretation of the tensions resulted from cooling. Nevertheless, it is clear that upon cooling, the tension in the vesicular membrane increases significantly.

Due to the tension in the membrane, the pressure profiles shift toward more negative local pressure values (see Fig. 1B). The largest changes are seen for the negative oil–water interfacial peaks. In case of the smallest vesicle, the magnitude of these peaks decreases from −35 to −105 bar in the inner monolayer and from −85 to −140 bar in the outer monolayer, a decrease by a factor of 2.9 and 1.6 respectively. The same trend is seen for the other vesicles, with relative changes by a factor of 2.1 and 1.7 in the inner monolayer and 1.8 and 1.5 in the outer monolayer for 30 and 40 nm diameter vesicles, respectively. These numbers demonstrate a clear trend toward a larger relative increase in stress in the inner monolayer compared to the outer monolayer of the vesicle, upon cooling of the vesicle below T_m.

3.2 Quenching of stressed planar membranes below T_m

To test the hypothesis that the effective area constraint on the liposomes prevents the formation of gel domains in these systems, as discussed in the previous section, here we look at the effect of area constraints on gel formation in planar membranes. To do so, we simulated small DPPC patches at a fixed area per lipid, covering a range of areas per lipid in between the gel and fluid phase. Each of these systems was quenched to a temperature of 273 K. In addition, we tested the effect of membrane asymmetry on gel phase formation by systematically removing lipids from one of the monolayers.

3.2.1 Area constraint induces fluid–gel phase coexistence in planar membranes. Fig. 2 shows graphical snapshots of the effect of an area constraint on a lamellar membrane, after a temperature quench from 323 K to 273 K. At an area per lipid of 0.64 nm^2, close to the equilibrium area per lipid at 323 K, the membrane remains completely in the L_α phase (Fig. 2A). Even when cooled to a temperature of 250 K, no gel formation was observed over a time period of 1 μs (results not shown). This finding indicates that the fluid phase at 273 K is most likely

Table 2 Properties of vesicles obtained from the pressure distribution

Vesicle diameter (nm)	R_{323K} [a] (nm)	R_{273K} [a] (nm)	ΔP_{323K} [b] (bar)	ΔP_{273K} [b] (bar)	σ_{323K} [c] (mN m^{-1})	σ_{273K} [c] (mN m^{-1})
20	8.0	7.8	8 ± 5	85 ± 5	4 ± 2	30 ± 6
30	12.3	12.2	19 ± 5	70 ± 5	13 ± 5	39 ± 8
40	16.6	16.3	22 ± 5	60 ± 5	14 ± 6	44 ± 9

[a] The radius is defined as the center of the positive peak of the carbon tails in the pressure profile. [b] Calculated as the difference in the pressure between the inside and outside of the vesicle. [c] The tensions were calculated using eqn (3).

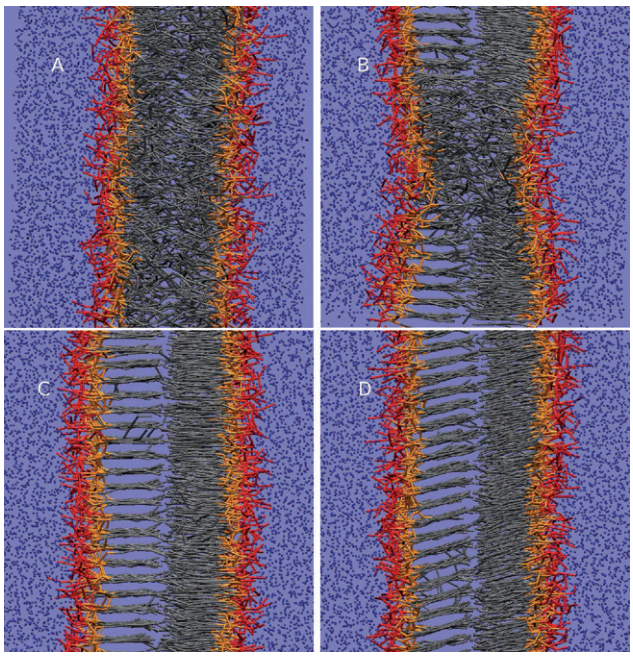

Fig. 2 Effect of an area constraint on DPPC bilayer patches cooled to 273 K. (A) An area per lipid of $A = 0.64$ nm^2, no gel formation is observed. (B) A = 0.54 nm^2, a gel domain is observed which is in coexistence with the fluid phase. (C) $A = 0.45$ nm^2, the entire membrane is in the gel phase. (D) An external tension of 90 mN m^{-1} applied to the membrane depicted in (C) leads to a tilted ($L_{\beta'}$) gel phase. Lipid head groups are depicted red, the glycerol groups orange, lipid tails grey, and water is shown as blue dots. Note that in all cases both monolayers are in the same phase; the gaps seen between the lipid tails in the gel phase in panels B–D depend on the viewing direction and only show up in one of the monolayers.

a stable state at this area per lipid. At an area of 0.54 nm^2, a gel domain spontaneously forms, reaching an equilibrium size after 100 ns with no further growth observed (Fig. 2B). Considering that a gel domain itself has a nearly fixed area per lipid, additional growth of the gel domain would further decrease the area per lipid of the surrounding fluid phase, with an associated cost in free energy (determined by the area compressibility modulus of the fluid phase). To optimize its free energy, the membrane therefore adopts a state of gel–fluid phase coexistence, finding a balance between the enthalpic gain of efficient lipid packing inside the gel phase and the elastic cost of increasing the area per lipid in the remaining fluid phase. The boundary interface between the two phases is straight and well-defined, reflecting a large line tension between the two phases. Upon further reduction of the area to 0.46 nm^2, the membrane is found to be entirely in the L_β gel phase (Fig. 2 C). An area per lipid of 0.46 nm^2 corresponds to the equilibrium area per lipid when no area constraint is present.

To quantify the appearance of the gel domains, we calculated the fraction of lipids in the gel phase as a function of the area. This is shown in Fig. 3, together with the associated surface tension of the membrane system. Three different regimes can be distinguished: *i*) *Fluid phase* (area per lipid > 0.59 nm^2). In this regime the area per lipid is so large that gel domains are not stable. The surface tension increases roughly linearly with the area per lipid, corresponding to the elastic behavior of a fluid

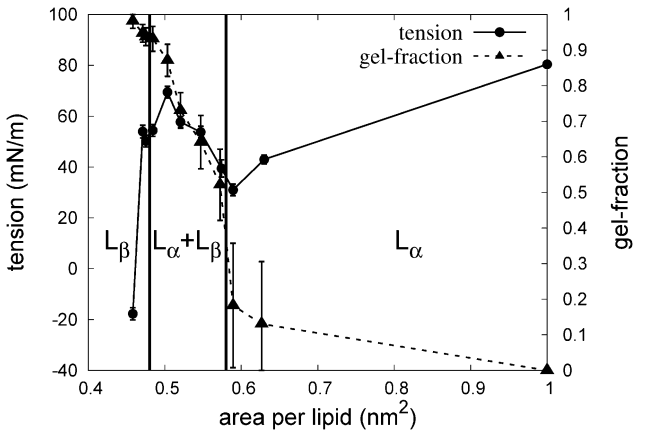

Fig. 3 Effect of an area constraint on the surface tension (solid line, circles) and on the fraction of gel phase (dotted line, triangles) of a DPPC bilayer cooled to 273 K.

bilayer. The increase in gel fraction to a value of 0.2 merely reflects the noise in the cluster algorithm used. Visual inspection shows that no actual gel domains are formed. *ii*) *Fluid–gel phase coexistence* (area per lipid 0.47–0.57 nm^2). Here, the L_α phase coexists with the L_β phase in the membrane. The surface tension increases inelastically with decreasing area per lipid and reaches a maximum value of 70 mN m^{-1} at an area per lipid of 0.50 nm^2. The L_β fraction on the other hand, increases gradually with decreasing area per lipid. The domain formation is reversible in this regime, *i.e.* an increase in area per lipid decreases the L_β fraction (results not shown). *iii*) *Gel phase* (area per lipid $\approx$ 0.46 nm^2). In this regime the tension rapidly decreases upon a minor decrease in area per lipid, reflecting the reduced compressibility of the gel phase with respect to the fluid phase. This regime, however, appears to be an irreversible regime; an external applied tension of 90 mN m^{-1} leads to a tilted gel phase ($L_{\beta'}$) rather than a decrease in the L_β fraction (*cf.* Fig. 2D).

Comparing the maximum area per lipid at which gel domains are stable in the planar membrane, around 0.57 nm^2, to the area per lipid of the inner and outer monolayers of the cooled vesicle, 0.60 and 0.69 nm^2 respectively, we conclude that the area constraint is indeed the reason for the absence of gel domain formation in the vesicular case.

3.2.2 Membrane asymmetry decouples gel phase formation in the two monolayers. An important difference between planar systems and vesicles is the asymmetry between the monolayers. Previous simulations addressing gel phase formation in DPPC bilayers suggested a strong coupling of the gel domains between the two opposite leaflets.[4] A plausible mechanism for monolayer coupling is the presence of a small surface tension between the two leaflets when the two different phases are in contact.[36] The vesicular membrane, however, is asymmetric. The two monolayers are structurally different[10] and it is therefore plausible that domain formation is less coupled between the monolayers when curvature is present. In order to isolate the effect of monolayer asymmetry, we investigated the formation of gel phase in asymmetric lamellar bilayers. We did so by systematically removing lipids from one of the monolayers of an equilibrated DPPC bilayer at 323 K, followed by lowering of the temperature

to 273 K. The simulations were performed under constant pressure conditions (see the Methods section), allowing the area per lipid to adjust to the low-temperature condition.

Fig. 4A shows the gel fraction in each monolayer as a function of the membrane asymmetry (expressed as the ratio between the number of lipids in each of the two monolayers). Monolayer 'I' denotes the normal monolayer, monolayer 'II' the depleted one. It can be seen that monolayer 'I' remains purely in the gel phase over the entire asymmetry range, whereas for the depleted monolayer the appearance of gel domains is observed at an asymmetry ratio of 0.8, with a complete transformation at 0.95. Below an asymmetry ratio of 0.8, the depleted monolayer remains in a fluid phase. At the asymmetry ratio of 0.8, the area per lipid in the depleted monolayer is 0.57 nm^2. Also, in the case of the symmetric bilayer simulated at constant area, gel phase formation was first observed at this area per lipid (*cf.* Fig. 3). It appears, therefore, that the effect of lipid asymmetry itself does not have an important effect on the onset of gel phase formation in planar membranes, other than the associated effect of an area constraint. However, a small but interesting difference between the asymmetric bilayer and the bilayer at constant area is noticeable. At the 'critical' area per lipid of 0.57 nm^2, 77% of the depleted monolayer is in the gel phase in the asymmetric bilayer, compared to only 53% in the symmetric case (equal for both monolayers). We attribute this apparent larger stability of the gel phase in the asymmetric system to the registration of the gel domains. In the asymmetric bilayer, the gel domain in the depleted monolayer is opposing a monolayer completely in the gel phase, whereas in the symmetric bilayer it faces a monolayer containing a fluid domain. This mismatch increases the inter-monolayer surface tension,[36] and hence suppresses further growth of the gel domains.

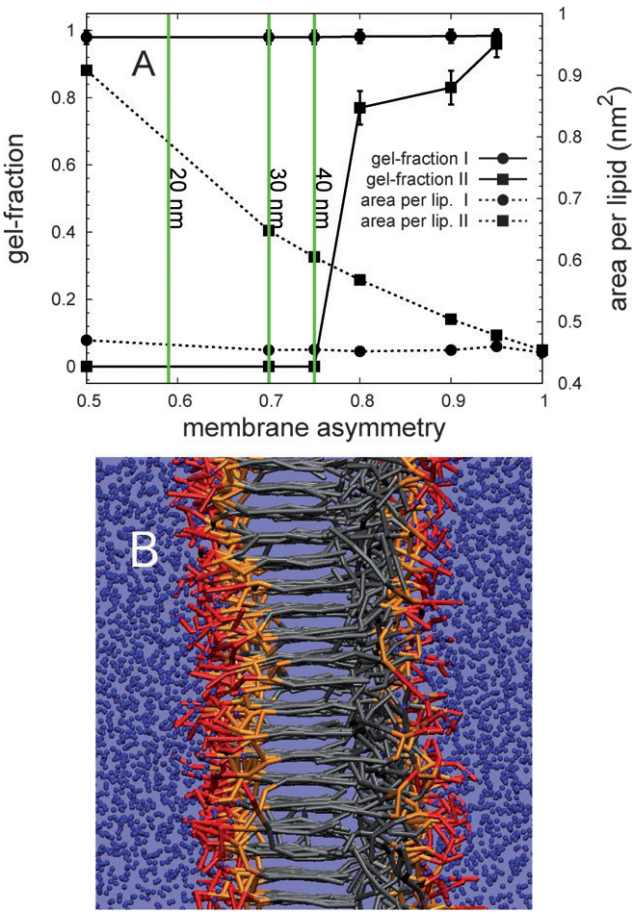

Fig. 4 Gel phase formation in asymmetric DPPC bilayers. (A) Gel fraction (solid lines) and area per lipid (dotted lines) for each monolayer, as a function of membrane asymmetry (expressed as ratio between the number of lipids in the two monolayers). Squares represent the monolayer depleted in lipids (II) and circles represent the normal monolayer (I). The green vertical lines are indicative of the membrane asymmetry in the three vesicles of 20, 30, and 40 nm. (B) Snapshot of a system at 273 K after 800 ns of simulation, with 50% of the lipids removed from the right monolayer (*i.e.* asymmetry ratio 0.5). The left monolayer is completely in the gel state (L_β) while the right monolayer remains completely in the fluid state (L_α). Lipid head groups are depicted red, the glycerol groups orange, lipid tails grey, and water is shown as blue dots.

3.3 Quenching vesicles below T_m under pseudo-equilibrium conditions

In this section, we describe results obtained for the same series of vesicular systems as before, with one important difference: artificial pores are present which allow for solvent exchange and lipid flipping in the cooled vesicle system. This approach releases the area constraint of the vesicular membrane, and mimics gel phase formation under pseudo-equilibrium conditions. Indeed, spontaneous gelation of the vesicles is observed in these set of simulations (denoted 'set 2' in Table 1). We will focus in detail on the domain formation in the smallest (20 nm diameter) vesicle simulated. Qualitatively similar results were obtained for the larger vesicles.

3.3.1 The four stages of gel formation in lipid vesicles. The gel formation process is found to proceed through four distinct stages, which become apparent from a plot of the gel-fraction *versus* simulation time, shown in Fig. 5 (lower panel). We discuss these regimes now in their order of appearance.

Stage A: Formation of uncoupled gel domains in the outer monolayer. The first stage is defined by the appearance of uncoupled gel domains in the outer monolayer only. In case of the 20 nm vesicle, this stage corresponds to, approximately, the first 250 ns of the simulation (*cf.* lower panel of Fig. 5). Fig. 6A shows a snapshot of such a decoupled gel domain in the 20 nm vesicle, 160 ns after the temperature quench. In line with the results obtained for the asymmetric planar membranes presented in the previous section (*cf.* Fig. 4), the gel domain is only present in the outer monolayer. The local curvature in the membrane is almost unaffected by the presence of these uncoupled gel domains, which is obvious from the graphical image (Fig. 6A) and is also revealed by the nearly constant asphericity parameter during stage A, shown in the upper panel of Fig. 5. During stage A, the internal volume of the vesicle has decreased by ~10% compared to the start of the simulation (*cf.* upper panel of Fig. 5). The pressure difference ΔP at this point is still considerable, around 70 bar, resulting in an estimated surface tension of 26 ± 5 mN m^{-1} using eqn (3). It should however be noted, that tension increases with decreasing area per lipid during the fluid–gel coexistence regime, as shown in Fig. 3 for the planar

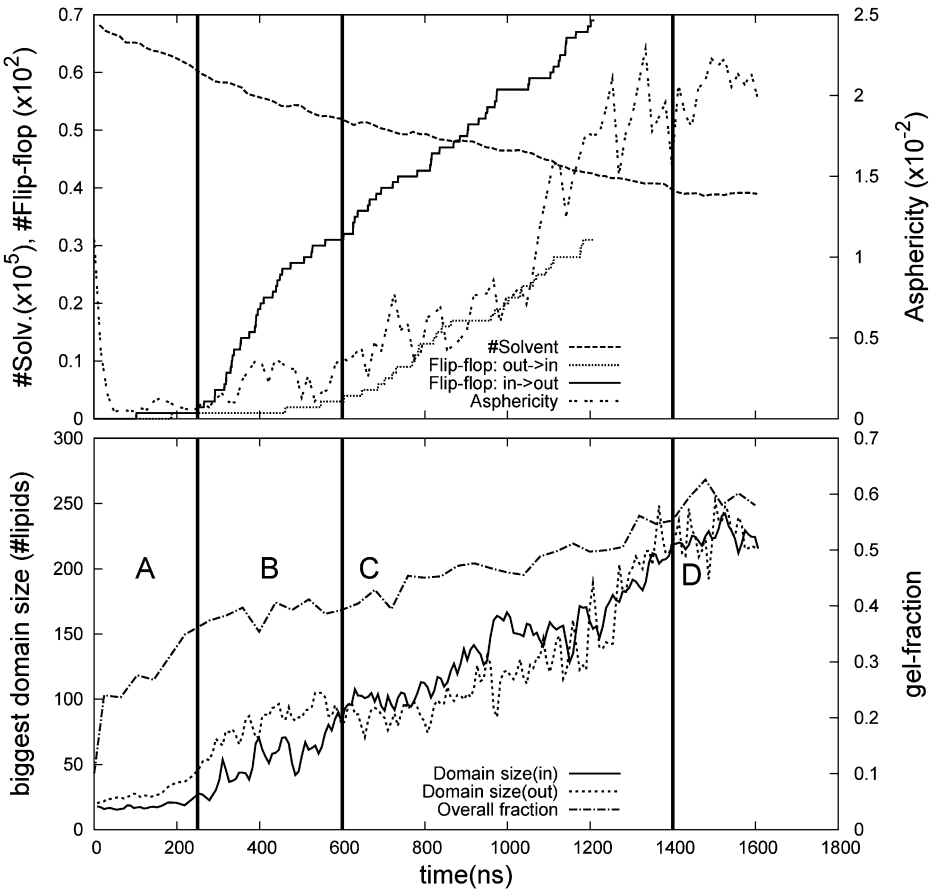

Fig. 5 Quantitative analysis of the evolution of domain formation in the 20 nm DPPC vesicle as a function of time. Upper panel: the amount of internal solvent particles, the amount and direction of lipid flip-flops and the asphericity parameter. Lower panel: size of the biggest domain in each monolayer, and the overall membrane fraction in the gel-phase. Due to the increasing asphericity of the vesicle and the existence of an 'offset time' in the definition of flip-flops, flip-flops could only be well defined between 200–1200 ns. The four different stages (A–D) are indicated; see the discussion in the main text.

membrane. Eqn (3) is in fact only applicable to radially homogeneous systems; the estimate of membrane tension during the freezing transition should therefore be considered qualitative. More informative is the area per lipid. The area per lipid at the position of the second tail bead (C2) is 0.67 nm^2 for the inner monolayer and 0.55 nm^2 for the outer monolayer. The latter value is already smaller than the 'critical' area per lipid of 0.57 nm^2 found for the planar bilayer, *i.e.*, the area per lipid for which gel domains were found to be stable in planar bilayers. These values suggest that it is especially the local available space of the tail beads that plays a crucial role in triggering the phase transition, and explains why gel domains appear in the outer monolayer first.

Stage B: Gel domain formation in the inner monolayer. The second stage in the evolution of the phase transition is the initiation of domain formation in the inner monolayer. With reference to the lower panel of Fig. 5, stage B covers the time period roughly between 250 and 600 ns. During this period, the size of the largest gel domain in the outer monolayer reaches a plateau. Thus, while the further growth of the outer monolayer gel fraction is limited, the inner monolayer catches up. We explain this observation by three possible factors that come into play. The first factor is the inter-monolayer surface tension. Based on our results obtained for planar bilayers, discussed in the previous section, we expect the growth of an uncoupled gel domain to be energetically unfavorable due to the surface tension between a gel domain in one monolayer facing a fluid phase in the opposing leaflet. A second factor, and probably more important one, is the reduced area per lipid of the gel domain with respect to the fluid phase. Although the total area of the outer monolayer is no longer constrained (due to the presence of the pores), the relative change in area between the two monolayers requires lipid flip-flopping. Due to the presence of the pores, flip-flopping of lipids is actually possible, yet it is a process that is much slower than the efflux of solvent. Formation of gel domains puts the outer monolayer therefore under stress, reducing further growth of the domains similar to that observed for the planar membranes under stress (*cf.* Fig. 3). Related to this is a third factor, which is the larger transmonolayer asymmetry associated with a smaller vesicle. As shown in our previous work,[15] vesicles with smaller radii are relatively enriched in lipids in the outer monolayer. Again, this requires lipid flip-flopping. Fig. 5 (top panel) shows the onset of this process, with a large number of lipid flip-flops taking place during this stage, enriching the lipid population of the outer monolayer. Note that the detection of the flip-flops involves a lag-time (see Methods section); it is likely that the onset of lipid flip-flopping already starts during the previous

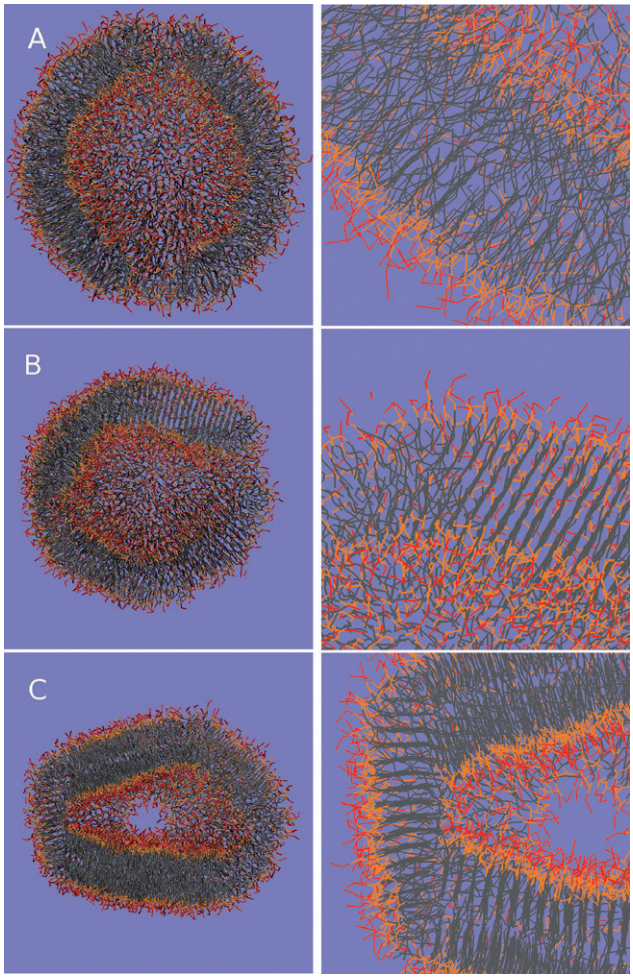

Fig. 6 Snapshots from the cross-section of the 20 nm diameter vesicle during different stages of the evolution of domain formation (*cf.* Fig. 5). (A) Left, stage A after 160 ns, the first gel domains have appeared in the outer monolayer of the vesicle. The shape of the vesicle remains nearly unaffected. Right, zoomed view of the uncoupled gel-domain during this stage. (B) Left, stage C at 600 ns, the gel domains in the opposing monolayers are coupled. Some clear 'kinks' are appearing in the membrane. Right, close-up of the coupled gel domain. (C) Left, stage D at 1400 ns, an equilibrium situation where the gel domains have reached their maximum size. The vesicle has become very irregular, with an egg-shaped cross-section. Right, close-up of the cross-section of the 'tip' of the vesicle. Lipid head groups are depicted red, the glycerol groups orange, lipid tails grey, and water is omitted for clarity.

stage. During stage B, the area per lipid in the inner monolayer remained more or less constant (around 0.62 nm^2, data not shown). This phenomenon results from two opposing effects, namely the general shrinking of the vesicle on the one hand, and the lipid depletion of the inner monolayer, through flip-flops, on the other. It is interesting that gel domains nevertheless are formed in the inner monolayer, despite the fact that the area per lipid is still above the threshold value of 0.57 nm^2.

Stage C: Coupled growth of gel domains and vesicle deformation. Once the process of 'catching up' of gel domain formation in the inner monolayer has occurred during stage B, the speed of gel domain growth in both monolayers becomes similar. This can be concluded from Fig. 5, showing the growth of the gel domains to be strongly correlated between the monolayers. In addition, the lipid flip-flop rate becomes similar in both directions, *i.e.* no further enrichment of the outer monolayer occurs. This stage lasts approximately from 600 to 1400 ns, ending with the stabilization of the gel domain sizes and overall gel fraction. From the top panel of Fig. 5, a strong increase in the asphericity parameter can be appreciated during stage C. This is likely caused by the increased bending stiffness of the membrane as a result of the increasing size of coupled gel domains. The inability of these gel domains to adjust to the large vesicle curvature results in a strong deformation of the vesicle. A snapshot of the vesicle during this stage is shown in Fig. 6B. Remarkably, the pressure difference between the vesicle interior and exterior is still substantial, around 50 bar on average during stage C.

Stage D: Stabilization of fluid–gel coexistence. After 1400 ns, the domain growth of the 20 nm vesicle appears to have reached a plateau (*cf.* Fig. 5). At this stage the vesicular membrane has stabilized into a state of fluid–gel coexistence, with around 60% of the membrane in the gel phase and 40% in the fluid phase. At the final point of the simulation (after 1600 ns), the vesicle contains around 3900 internal solvent beads, which is a 45% decrease of internal volume compared to the initial conditions. Experimentally, a reduction of between 25%–30% has been determined for a DPPC vesicle 70 nm in diameter.[37] Although a direct comparison is not possible, both simulation and experiment reveal a substantial decrease in internal solvent volume accompanying the gelation process. At the end of our simulation, no more net solvent flux occurs through the pores, and the pressure difference has fully relaxed ($\Delta P = 0$). The pores sealed when the cylindrical potentials were removed (not shown), implying little or no remaining tension. Fig. 6C reveals how intriguing the organisation in lipid packing is in order to accommodate the stress imposed by the curved nature of a small vesicle. The final shape of the vesicle resembles that of an egg. The curvature at the 'tip' of the egg is so large that in fact almost no inner monolayer is present. The outer monolayer at the tip is completely in the gel phase, and is oriented almost perpendicularly with respect to the surrounding gel domains. At the interface between the tip domain and the 'body' of the vesicle, the gel domains are connected by lipids remaining in the fluid phase (most clearly visible in the outer monolayer; see right panel of Fig. 6C). The packing of the lipids in the gelated vesicle is somewhat reminiscent of that seen in the rippled gel phase.[7]

3.3.2 Freezing induced vesicle rupture. Qualitatively similar stages were observed for the freezing of the somewhat larger vesicles. We did not analyze this process in so much detail compared to the 20 nm vesicle, mainly because the accessible time scale (300 ns for the 40 nm vesicle) was not sufficient to reach an equilibrated state. However, an interesting additional effect was observed for the 40 nm vesicle. As shown in Fig. 7, the radius of the artificial pore spontaneously increased during the freezing process. The widening of the pore already took place during the first stage of the cooling, stabilizing to a pore with a radius of about 8 nm after 160 ns (recall that the radius of the original pore was 3.5 nm). The increase in pore size indicates that the rupture threshold of the membrane is surpassed, causing the

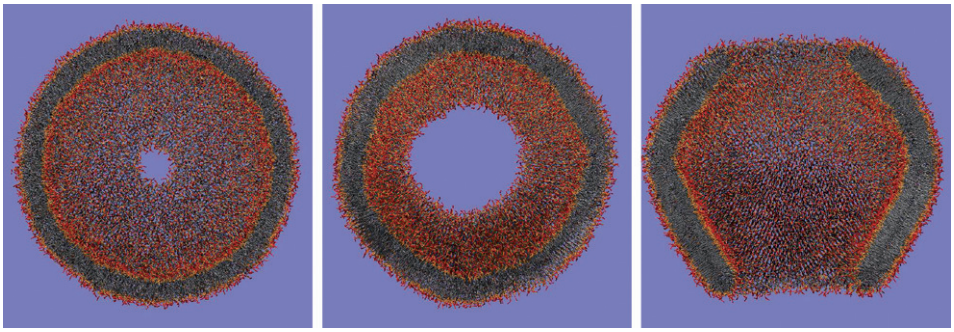

Fig. 7 Snapshots showing the cooling of a 40 nm diameter vesicle from 323 K to 273 K. Cross-sections through the middle of the vesicle are shown. From left to right: (1) The starting situation, showing one out of two hydrophilic pores of 3.5 nm radius which were artificially induced from the start. The entire vesicle is in the fluid state. (2) The situation after 160 ns. The pore size has increased to a 8 nm radius. Gel domains coupled across the monolayers have already formed. (3) A cross-section of the same vesicle as shown in (B), viewed along the direction of the pores. Both pores are of similar size. Kinks in the contour are clearly visible, and indicate the connections between different gel patches. Lipids in the vicinity of the kinks as well as around the pore interfaces remain in the fluid state. Lipid head groups are depicted red, the glycerol groups orange, lipid tails grey, and water is omitted for clarity.

vesicle to pop like a balloon. The rupturing process observed in our simulations might be similar to the freezing-induced rupture of liposomes found experimentally.[38,39]

3.3.3 Solvent efflux is the main kinetic barrier for gel phase formation in vesicles. Finally, we wish to re-address the question of whether it is the ability to release the interior solvent pressure, or the ability to remove the stress imbalance between the monolayers through lipid flip-flops, that allows the vesicles to undergo the transformation to the gel phase. To this end, we cooled another 20 nm vesicle without the artificial presence of pores, but with the initial reduction of internal solvent to 3900 CG solvent beads (corresponding to the final solvation state of the porated 20 nm vesicle, *cf.* Fig. 5). This simulation proceeded through the same stages as observed during the simulation in which the artificial pores were present (discussed before). The final stage shows a strongly deformed vesicle, similar to the one shown in Fig. 6, with large gel domains coupled between the monolayers. It appears, therefore, that the ability to expel interior solvent after the instantaneous cooling of the vesicles is of primary importance for gel formation to occur. However, the gel fraction was in this case 11% lower than the vesicle where artificial pores were used, which we attribute to the lack of lipid flip-flop-mediated stress minimization.

4 Conclusions

Using a model at near-atomic resolution, we have been able to shed some light on the kinetic and structural aspects of gel domain formation in small lipid vesicles. Cooling 20–40 nm sized vesicles below the main phase transition temperature does not lead to gel phase formation on the microsecond time scale. Based on control simulations of planar membrane systems, we conclude that this is caused by the implicit area constraint of the liposomal membrane as a consequence of its very low water permeability at low temperature. To mimic the long time scale effect, we introduced artificial pores which allow both the exchange of internal solvent and the ability of lipids to redistribute between the two monolayers. In this case the transformation from a fluid to a gel phase vesicle could be observed. Four different stages were identified during the transformation. The first stage is characterized by the formation of gel domains in the outer monolayer only. In the second stage, the outer domain growth is strongly reduced, however, domains start forming in the inner monolayer. In the third stage, domains become coupled across the monolayers, and the gel fraction increases for both monolayers. During this stage the vesicles also start to deform considerably. Eventually, an equilibrium stage is reached with most of the lipids in the gel state. For a 20 nm diameter vesicle, the equilibration process requires about a microsecond. The finally obtained gelated vesicles are very irregularly shaped, with planar gel domains joined together in a kinked geometry, separated by domain–domain interfaces of lipids in the fluid phase. For the largest vesicles studied (around 40 nm diameter), we observed spontaneous membrane rupture during the phase transformation. Control simulations with a pre-deflated vesicle again underlined the importance of solvent exchange. We conclude that rapid solvent efflux is the major kinetic barrier for gel phase formation in instantaneously cooled vesicles, at least on a nanosecond to microsecond time scale.

5 Acknowledgements

This work was supported by the Netherlands Organisation for Scientific Research (NWO) through the Molecule-To-Cell program and a TOP-grant. We also acknowledge useful discussions with Alan Mark.

6 References

1 R. L. Biltonen and D. Lichtenberg, *Chem. Phys. Lipids*, 1993, **64**, 129–142.
2 R. Koynova and M. Caffrey, *Biochim. Biophys. Acta*, 1998, **1376**, 91–145.
3 G. Strauss and H. Hauser, *Proc. Natl. Acad. Sci. U. S. A.*, 1986, **83**, 2422–2426.
4 S. J. Marrink, H. J. Risselada and A. E. Mark, *Chem. Phys. Lipids*, 2005, **135**, 223–244.
5 O. G. Mouritsen, A. Boothroyd, R. Harris, N. Jan, T. Lookman, L. MacDonald, D. A. Pink and M. J. Zuckermann, *J. Chem. Phys.*, 1983, **79**, 2027–2041.
6 R. Jerala, P. F. Almeida and R. L. Biltonen, *Biophys. J.*, 1996, **71**, 609–615.

7 A. H. de Vries, S. Yefimov, A. E. Mark and S. J. Marrink, *Proc. Natl. Acad. Sci. U. S. A.*, 2005, **102**, 5392–5396.
8 S. S. Qin, Z. W. Yu and Y. Yu, *J. Phys. Chem. B*, 2009, **113**, 8114–8123.
9 S. Leekumjorn and A. K. Sum, *J. Phys. Chem. B*, 2007, **111**, 6026–6033.
10 S. J. Marrink and A. E. Mark, *J. Am. Chem. Soc.*, 2003, **125**, 15233–15242.
11 P. M. Kasson, N. W. Kelley, N. Singhal, M. Vrljic, A. T. Brunger and V. S. Pande, *Proc. Natl. Acad. Sci. U. S. A.*, 2006, **103**, 11916–11921.
12 J. C. Shillcock and R. Lipowsky, *Nat. Mater.*, 2005, **4**, 225–228.
13 V. Knecht and S. J. Marrink, *Biophys. J.*, 2007, **92**, 4254–4261.
14 A. J. Markvoort, K. Pieterse, M. N. Steijaert, P. Spijker and P. A. J. Hilbers, *J. Phys. Chem. B*, 2005, **109**, 22649–22654.
15 H. J. Risselada and S. J. Marrink, *Phys. Chem. Chem. Phys.*, 2009, **11**, 2056–2067.
16 G. Ayton, A. M. Smondyrev, S. G. Bardenhagen, P. McMurtry and G. A. Voth, *Biophys. J.*, 2002, **83**, 1026–1038.
17 M. Laradji and P. B. S. Kumar, *J. Chem. Phys.*, 2005, **123**, 224902.
18 H. J. Risselada and S. J. Marrink, *Proc. Natl. Acad. Sci. U. S. A.*, 2008, **105**, 17367–17372.
19 S. J. Marrink, A. H. de Vries and A. E. Mark, *J. Phys. Chem. B*, 2004, **108**, 750–760.
20 S. J. Marrink, H. J. Risselada, S. Yefimov, D. P. Tieleman and A. H. de Vries, *J. Phys. Chem. B*, 2007, **111**, 7812–7824.
21 S. J. Marrink and A. E. Mark, *Biophys. J.*, 2004, **87**, 3894–3900.
22 A. H. de Vries, A. E. Mark and S. J. Marrink, *J. Am. Chem. Soc.*, 2004, **126**, 4488–4489.
23 O. H. S. Ollila, H. J. Risselada, M. Louhivuori, E. Lindahl, I. Vattulainen and S. J. Marrink, *Phys. Rev. Lett.*, 2009, **102**, 078101.
24 H. J. Risselada, A. E. Mark and S. J. Marrink, *J. Phys. Chem. B*, 2008, **112**, 7438–7447.
25 A. J. Markvoort, P. Spijker, A. F. Smeijers, K. Pieterse, R. A. van Santen and P. A. Hilbers, *J. Phys. Chem. B*, 2009, **113**, 8731–8737.
26 H. J. C. Berendsen, J. P. M. Postma, W. F. van Gunsteren, A. Di Nola and J. R. Haak, *J. Chem. Phys.*, 1984, **81**, 3684–3690.
27 D. Van der Spoel, E. Lindahl, B. Hess, G. Groenhof, A. E. Mark and H. J. C. Berendsen, *J. Comput. Chem.*, 2005, **26**, 1701–1718.
28 S. E. Feller, Y. Zang, R. W. Pastor and B. R. Brooks, *J. Chem. Phys.*, 1995, **103**, 4613–4621.
29 H. Heller, M. Schaefer and K. Schulten, *J. Phys. Chem.*, 1993, **97**, 8343–8360.
30 S. M. Thompson, K. E. Gubbins, J. P. Walton, R. A. Chantry and J. S. Rowlinson, *J. Chem. Phys.*, 1984, **81**, 530–542.
31 A. Carruthers and D. L. Melchior, *Biochemistry*, 1983, **22**, 5797–5807.
32 J. Andrasko and S. Forsen, *Biochem. Biophys. Res. Commun.*, 1974, **60**, 813–819.
33 D. Lide, *Handbook of Chemistry and Physics*, 72nd edition, 1991–1992.
34 E. Evans and V. Heinrich, *C. R. Phys.*, 2003, **4**, 265–274.
35 H. Leontiadou, A. E. Mark and S. J. Marrink, *Biophys. J.*, 2004, **86**, 2156–2164.
36 M. D. Collins, *Biophys. J.*, 2008, **94**, L32–L34.
37 D. Lichtenberg, P. L. Felgner and T. E. Thompson, *Biochim. Biophys. Acta, Biomembr.*, 1982, **684**, 277–281.
38 L. M. Hays, J. H. Crowe, W. Wolkers and S. Rudenko, *Cryobiology*, 2001, **42**, 88–102.
39 L. T. Boni, S. R. Minchey, W. R. Perkins, P. L. Ahl, J. L. Slater, M. W. Tate, S. M. Gruner and A. S. Janoff, *Biochim. Biophys. Acta, Biomembr.*, 1993, **1146**, 247–257.